Vibrational Spectroscopy of Conducting Polymers: Fundamentals and Applications

Yukio Furukawa
Waseda University, Tokyo, Japan

1 INTRODUCTION

The conducting and semiconducting properties of organic polymers such as polyacetylene, polythiophene, poly(*p*-phenylene), poly(*p*-phenylenevinylene), etc. (Figure 1) have been studied extensively, because they can be used as active materials in flexible and low-cost electronic devices such as light-emitting diodes (LEDs), field-effect transistors (FETs), and solar cells.[1–4] These properties arise from conjugated π-electrons. Conjugated polymers are organic semiconductors whose band gaps are typically in the range from 1 to 3 eV. A conjugated polymer can be doped chemically with an electron acceptor such as one of the halogens to give, for example, AsF_5, and $FeCl_3$, or an electron donor such as an alkali metal. The chemical doping is performed by exposing a polymer film in various ways to an acceptor or a donor. The main process of doping is a redox reaction between the polymer chains and the acceptor or donor. Upon acceptor doping (p-type doping), an ionic complex consisting of multiply oxidized (positively charged) polymer chains and counter anions (e.g., I_3^-, AsF_6^-) is formed. Counter anions are generated by reduction of acceptors. In the case of donor doping (n-type doping), an ionic complex consisting of multiply reduced (negatively charged) polymer chains and counter cations (e.g., Na^+, K^+) is formed. Counter cations are generated by oxidation of donors. The electrical conductivity of the polymer increases with increasing content of the dopant. At a heavily doped state, it shows metallic properties. Since the electrical conductivity (i.e., the Fermi level) of a conjugated polymer can be controlled by the content of a dopant, conjugated polymers can be used as organic semiconductors or metals. Doping also can be performed electrochemically.

It has been demonstrated that conjugated polymers can be used for FETs,[5,6] solar cells,[7] and LEDs,[8,9] as organic semiconductors. The properties of conjugated polymers have been interpreted by new concepts of elementary electronic excitations such as solitons,[10] polarons,[11–13] and bipolarons.[12–14] Since they can move along a polymer chain or hop between chains, they are also called quasi-particles. Charged excitations such as charged solitons, polarons, and bipolarons are charge carriers. Charge carriers can be generated by light irradiation and injection in junction structures. These new techniques in carrier

Vibrational Spectroscopy of Polymers: Principles and Practice. Edited by Neil J. Everall, John M. Chalmers and Peter R. Griffiths. ISBN: 978-0-470-01662-6.

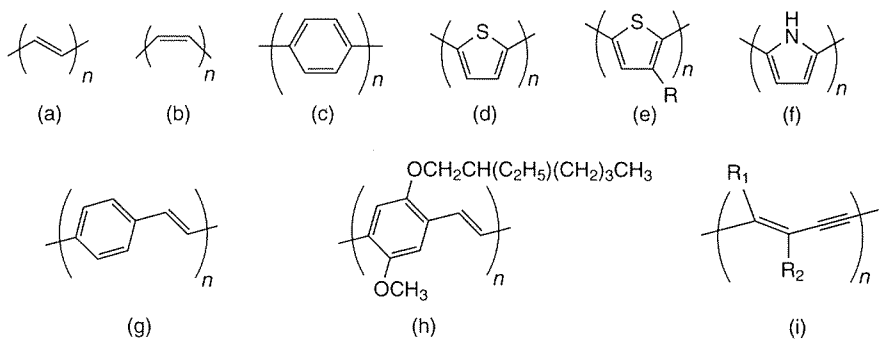

Figure 1. Chemical structures of conjugated polymers: (a) *trans*-polyacetylene; (b) *cis*-polyacetylene; (c) poly(*p*-phenylene); (d) polythiophenes; (e) regioregular poly(3-alkylthiophene); (f) polypyrrole; (g) poly(*p*-phenylenevinylene); (h) poly(2-methoxy-5-(2′-ethylhexyloxy)-*p*-phenylenevinylene) (MEH-PPV); (i) polydiacetylene. [Reproduced from Yukio Furukawa, 'Vibrational Spectroscopy of Conducting Polymers', in "Handbook of Vibrational Spectroscopy", eds J.M. Chalmers and P.R. Griffiths, John Wiley & Sons, Chichester, 2483–2495, Vol. 4 (2002).]

generation are used for transistors, light-emitting diodes, photovoltaic cells, etc.

Conjugated polymers can be classified into degenerate and non-degenerate polymers, according to the degeneracy of the ground states. The prototype of degenerate polymers is *trans*-polyacetylene (Figure 1(a)), which has a simple structure with alternating C=C and C−C bonds. The energy curve of *trans*-polyacetylene has two equal minima, where the alternating C=C and C−C bonds are reversed. On the other hand, a non-degenerate polymer has no two identical structures in the ground state. Most conjugated polymers belong to this class. The types of elementary excitations depend on the degeneracy of ground states. When an electron is removed from a non-degenerate polymer such as polythiophene (Figure 1(d)), charge $+e$ and spin 1/2 are localized over several repeating units with structural changes, as shown schematically in Figure 2(a). This is called a positive polaron. Since a positive polaron has charge $+e$ and spin 1/2, it corresponds to a radical cation in chemical terminology. When another electron is removed from the positive polaron, charge $+2e$ is localized over several units, as shown in Figure 2(b). This species is called a positive bipolaron, which has charge $+2e$ and no spin. Bipolarons are spinless carriers. In chemical terminology, a positive bipolaron corresponds to a dication. If a bipolaron is unstable, two polarons are formed. In the case of donor doping, a negative polaron and a negative bipolaron can be formed. In a degenerate polymer such as *trans*-polyacetylene, solitons can be formed. Solitons are classified into neutral, positive, and negative types according to their charges. A neutral soliton has no charge and spin 1/2 (Figure 2(c)). A positive soliton has charge $+e$ and no spin (Figure 2(d)). A negative soliton has charge $-e$ and no spin. Charged solitons are spinless carriers. A neutral soliton, a positive soliton, and a negative soliton correspond to the neutral radical, the cation, and the anion of a linear *trans*-oligoene with an odd number of carbon atoms, respectively. Although the charge and/or spin are depicted as being localized on one carbon atom in Figure 2(a–d), it should be noted that they extend over several rings with structural changes in real polymers. Elementary excitations in conjugated polymers are listed in Table 1, together with corresponding chemical terms. Since these excitations are associated with structural changes, they are also called self-localized excitations.

Actual samples of conjugated polymers have differing levels of sp^3 defects and a distribution of conjugation lengths. The structures of neutral conjugated polymers (e.g., conformations, configurations, conjugation length, defects) can

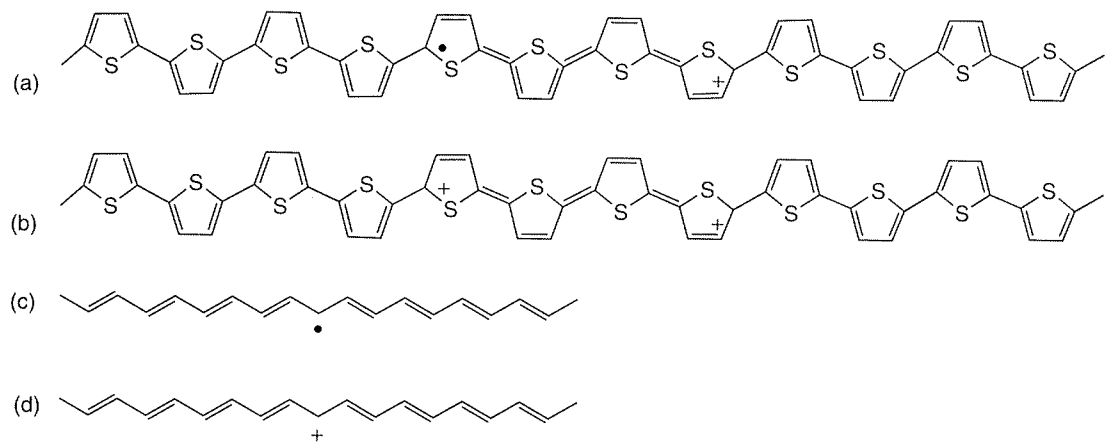

Figure 2. Schematic structures of elementary excitations: (a) a positive polaron; (b) a positive bipolaron; (c) a neutral soliton; (d) a positive soliton. [Reproduced from Yukio Furukawa, 'Vibrational Spectroscopy of Conducting Polymers', in "Handbook of Vibrational Spectroscopy", eds J.M. Chalmers and P.R. Griffiths, John Wiley & Sons, Chichester, 2483–2495, Vol. 4 (2002).]

Table 1. Elementary excitations in conjugated polymers and chemical terminology.

Elementary excitation	Chemical term	Charge	Spin
positive polaron	radical cation	$+e$	1/2
negative polaron	radical anion	$-e$	1/2
positive bipolaron	closed-shell dication	$+2e$	0
negative bipolaron	closed-shell dianion	$-2e$	0
neutral soliton	neutral radical	0	1/2
positive soliton	cation	$+e$	0
negative soliton	anion	$-e$	0

be obtained by Raman and infrared (IR) spectroscopy. Spectroscopic studies of well-defined oligomers are useful for a better understanding of the Raman and IR spectra of pristine polymers. Studies of the vibrational spectra of pristine conjugated polymers, and doping- and photo-induced IR absorption spectra, have been reviewed previously.[15–19] Electronic and vibrational spectra associated with the charge carriers generated by doping have been elucidated.[20–23] Thin polymer films have been used in organic LEDs and FETs. Carriers are associated with the functions of the devices. In this chapter, we will focus our attention on the vibrational spectroscopy of conjugated conducting polymers. We will describe the Raman and IR spectra of pristine polymers and carriers generated by chemical doping and light irradiation. We will also mention the Raman and IR studies on organic LEDs and FETs.

2 RAMAN AND IR SPECTRA OF PRISTINE POLYMERS

Totally symmetric modes are dominant in the observed Raman spectra of pristine conjugated polymers in most cases, and they reflect the effective conjugation length of the polymer chains.[15–19] In the IR spectra of pristine conjugated polymers, the CH out-of-plane bending vibrations, which are markers of geometrical isomerism or substituent positions of benzene rings or heterocycles, are observed strongly.[16,22,23]

2.1 Trans-polyacetylene

The Raman and IR spectra of *trans*-polyacetylene are shown in Figure 3(a) and (b), respectively.

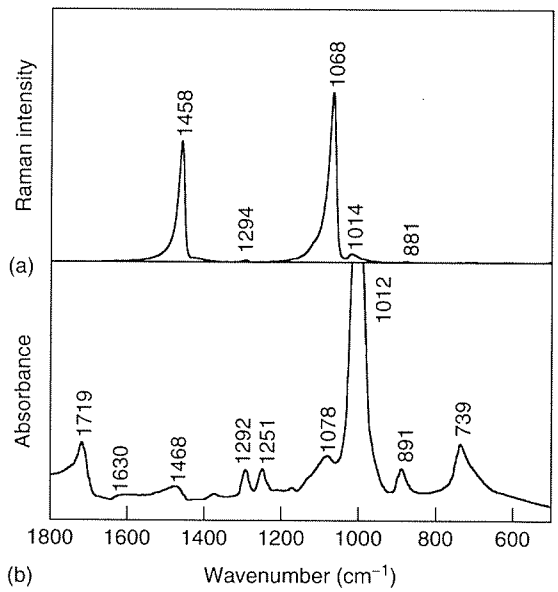

Figure 3. (a) Raman and (b) IR spectra of *trans*-polyacetylene. The Raman spectrum was taken with the excitation wavelength of 1064 nm. [Reproduced from Yukio Furukawa, 'Vibrational Spectroscopy of Conducting Polymers', in "Handbook of Vibrational Spectroscopy", eds J.M. Chalmers and P.R. Griffiths, John Wiley & Sons, Chichester, 2483–2495, Vol. 4 (2002).]

The Raman spectrum was recorded using excitation at 1064 nm. The vibrational spectra of *trans*-polyacetylene have been assigned on the basis of infinite planar structures for the first approximation. The vibrational irreducible representation at the zone center ($k = 0$) of a planar infinite *trans*-polyacetylene chain (C_{2h}) is as follows: $4a_g(R) + a_u(IR) + b_g(R) + 2b_u(IR)$.

The assignments of the vibrational spectra of *trans*-polyacetylene are listed in Table 2. There are five Raman-active modes, including one CH stretching, and three IR-active modes, including one CH stretching. The band assignments have been made on the basis of the wavenumber shifts on isotope substitution and normal coordinate calculations.[24–29] The Raman bands observed at 1458, 1294, and 1068 cm^{-1} are assigned to the $\nu_2(a_g)$, $\nu_3(a_g)$, and $\nu_4(a_g)$ modes, respectively. The 881-cm^{-1} Raman band is assigned to the $\nu_6(b_g)$ mode. The IR band

Table 2. Vibrational frequencies and assignments of *trans*-polyacetylene.

Species	No.	Calculated[28] (cm^{-1})	Observed (cm^{-1})	Mode
a_g	ν_1	–	–	CH str
	ν_2	1470	1458	C=C str
	ν_3	1302	1294	CC str
	ν_4	1079	1068	CH ip-bend
a_u	ν_5	1014	1012	CH op-bend
b_g	ν_6	887	881	CH op-bend
b_u	ν_7	–	3012	CH str
	ν_8	1235	1251	CH ip-bend

str, stretch; ip, in-plane; op, out-of-plane.

observed at 1251 cm^{-1} is assigned to the $\nu_8(b_u)$ mode. The intense IR band at 1012 cm^{-1} is characteristic of the CH out-of-plane wagging ($\nu_5(a_u)$) associated with *trans*-CH=CH groups. The assignments of weak bands are given in the papers reported by Takeuchi *et al.*[28] and Hirata *et al.*[29] The Raman spectrum of *trans*-polyacetylene has been explained by the effective conjugation coordinate (ECC) theory proposed by Castiglioni *et al.*[30] Their theory, which has been successfully applied to other conjugated polymers,[17,19] is a molecular spectroscopy version of the amplitude mode theory.[31,32] According to these theories, the vibrational modes that induce out of phase oscillations of alternate bonds have strong Raman intensities. The $\nu_2(a_g)$ and $\nu_4(a_g)$ vibrations strongly modulate the alternation of the antisymmetric stretching modes of C=C and C–C bonds. It is well known that the ν_2 and ν_4 Raman bands of *trans*-polyacetylene show changes in wavenumber and/or band shape with various excitation wavelengths. These observations reflect the coexistence of the segments having various effective conjugation lengths in a *trans*-polyacetylene film.

The Raman band observed at 1014 cm^{-1} has been assigned to the CH out-of-plane wagging, which is predicted to be IR active and Raman inactive, on the basis of the wavenumber shift on ^{13}C-substitution.[28] The appearance of the Raman-inactive mode in the Raman spectrum can be explained by the reduction of symmetry due to

the distortion of polyacetylene chains. Recently, helical polyacetylene has been synthesized by using chiral nematic liquid crystal solvents.[33]

2.2 Polythiophene

The Raman and IR spectra of polythiophene are shown in Figure 4(a) and (b), respectively. The observed bands have been explained by assuming a coplanar *s-trans* infinite structure (D_{2h}).[34–39] The vibrational irreducible representation at the zone center ($k = 0$) of the infinite chain is as follows: $7a_g(R) + 3a_u + 7b_{1g}(R) + 3b_{1u}(IR) + 3b_{2g}(R) + 6b_{2u}(IR) + 3b_{2g}(R) + 6b_{3u}(IR)$. The x-axis is taken along the polymer chain and the z-axis perpendicular to the polymer plane.

The assignments of the in-plane vibrations are listed in Table 3. The Raman bands observed at 1457, 1368, 1219, 1045, 700, and 301 cm^{-1} are assigned to the $\nu_2(a_g)$, $\nu_3(a_g)$, $\nu_4(a_g)$, $\nu_5(a_g)$, $\nu_6(a_g)$, and $\nu_7(a_g)$ modes, respectively. The 1493-cm^{-1} band is assigned to the $\nu_{12}(b_{1g})$ mode. The 1490- and 1440-cm^{-1} IR bands are assigned to the C=C antisymmetric stretching $\nu_{34}(b_{3u})$ and

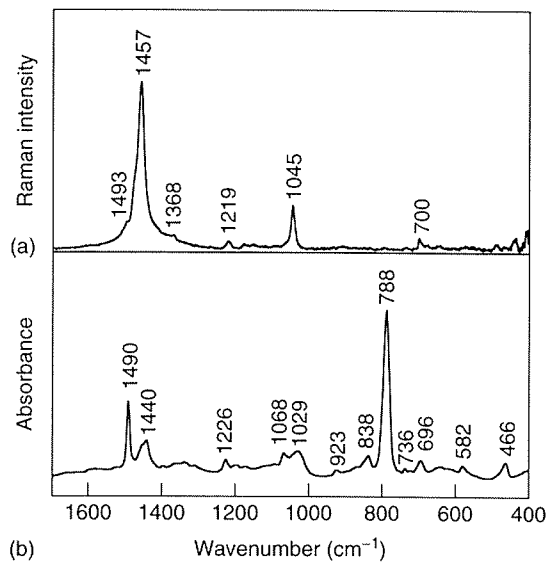

Figure 4. (a) Raman and (b) IR spectra of polythiophene. The Raman spectrum was taken with the excitation wavelength of 1064 nm.

Table 3. In-plane vibrational frequencies and assignments of polythiophene.

Species	No.	Calculated (cm^{-1})		Observed (cm^{-1})	Mode
		Ref. 36	Ref. 38		
a_g	ν_1	3094	3099	–	CH str
	ν_2	1475	1530	1457	C=C sym str, inter-ring CC str
	ν_3	1407	1386	1368	ring str
	ν_4	1229	1215	1219	ring str
	ν_5	1053	1057	1045	CH bend
	ν_6	708	707	700	ring deform
	ν_7	285	285	301	skeletal
b_{1g}	ν_{11}	3080	3082	–	CH str
	ν_{12}	1558	1591	1493	C=C antisym str, inter-ring CC str
	ν_{13}	1242	1289	–	ring str
	ν_{14}	1228	1250	–	CH bend
	ν_{15}	743	752	–	ring deform
	ν_{16}	504	516	–	skeletal
	ν_{17}	400	397	–	skeletal
b_{2u}	ν_{24}	3093	3099	3064	CH str
	ν_{25}	1418	1459	1440	C=C sym str
	ν_{26}	1295	1246	1226	ring str
	ν_{27}	1062	1072	1068	CH bend
	ν_{28}	864	844	838	ring str
	ν_{29}	602	600	582	ring deform
b_{3u}	ν_{33}	3078	3082	3064	CH str
	ν_{34}	1483	1495	1490	C=C antisym CC str
	ν_{35}	1171	1199	–	CH bend
	ν_{36}	917	917	923	ring str
	ν_{37}	749	758	736	ring deform
	ν_{38}	190	192	–	skeletal

str, stretch; deform, deformation; sym, symmetric; antisym, antisymmetric.

symmetric stretching $\nu_{25}(b_{2u})$ vibrations, respectively. The 788-cm^{-1} IR band is assigned to the CH out-of-plane wagging $\nu_{18}(b_{1u})$ of 2,5-disubstituted thiophene rings, and the 696-cm^{-1} band to the CH out-of-plane wagging of terminal 2-monosubstituted thiophene rings. Thus, the intensity ratio of these bands can be used as a marker of the degree of polymerization. The 466-cm^{-1} IR band is assigned to the out-of-plane bending vibration $\nu_{19}(b_{1u})$. The marker bands of distorted structures, conjugation length, etc. are

described in the review reported by Harada and Furukawa.[16] However, the complete assignment of all the observed bands has not yet been made.

2.3 Poly(p-phenylenevinylene)

The Raman and IR spectra of poly(*p*-phenylenevinylene) are shown in Figure 5(a) and (b), respectively. These spectra have been analyzed assuming a coplanar infinite polymer structure (C_{2h}).[40–42] The vibrational irreducible representation at the zone center ($k = 0$) of the infinite chain is as follows: $14a_g(R) + 6a_{xu}(IR) + 6b_g(R) + 12b_u(IR)$.

The observed spectra have been assigned on the basis of the experimental and calculated spectra of oligomers.[40–42] The assignments of the spectra are listed in Table 4. There are $14a_g$ modes, including three CH stretchings. The Raman bands observed at 1624, 1581, 1546, 1328, 1301, 1193, 1171, 886, 661, 634, and 328 cm^{-1} are assigned to the in-plane $\nu_4(a_g)$–$\nu_{14}(a_g)$ modes, respectively. The 959- and 860-cm^{-1} bands are assigned to the out-of-plane vibrations of $\nu_{21}(b_g)$ and $\nu_{22}(b_g)$, respectively. There are $12b_u$ modes that are infrared

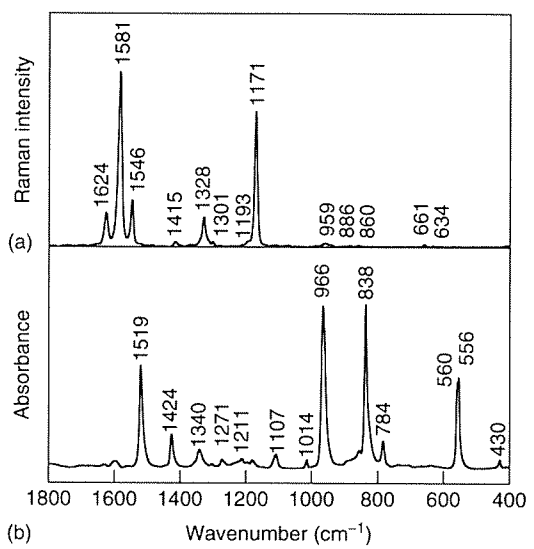

Figure 5. (a) Raman and (b) IR spectra of poly(*p*-phenylenevinylene). The Raman spectrum was taken with the excitation wavelength of 1064 nm.

Table 4. Vibrational frequencies and assignments of poly(*p*-phenylenevinylene).

Species	No.	Calculated (cm^{-1})	Observed (cm^{-1})	Mode
a_g	ν_1	3124	–	CH str
	ν_2	3099	–	CH str
	ν_3	3075	–	vinyl CH str
	ν_4	1650	1624	vinyl C=C str, ring str (8a)
	ν_5	1592	1581	ring str (8a), vinyl C=C str
	ν_6	1549	1546	ring str (8b)
	ν_7	1314	1328	vinyl CH ip-bend, CH ip-bend
	ν_8	1291	1301	CH ip-bend, vinyl CH ip-bend
	ν_9	1194	1193	C–C str
	ν_{10}	1163	1171	CH ip-bend (9a)
	ν_{11}	883	886	ring str (1), C–C str
	ν_{12}	644	661	ring ip-deform (6b)
	ν_{13}	632	634	ring ip-deform (6a)
	ν_{14}	293	328	rotational
a_u	ν_{15}	980	966	vinyl CH op-bend
	ν_{16}	957	–	CH op-bend (17a)
	ν_{17}	840	838	CH op-bend (11)
	ν_{18}	558	556	ring op-deform (16b)
	ν_{19}	403	–	ring op-deform (16a)
	ν_{20}	220	–	skeletal op-deform
b_g	ν_{21}	960	959	CH op-bend (5)
	ν_{22}	880	860	vinyl CH op-bend
	ν_{23}	820	–	CH op-bend (10a)
	ν_{24}	706	–	skeletal op-deform (4)
	ν_{25}	313	–	rotational
	ν_{26}	107	–	skeletal op-deform
b_u	ν_{27}	3122	3110	CH str
	ν_{28}	3097	3077	CH str
	ν_{29}	3082	3024	vinyl CH str
	ν_{30}	1517	1519	ring str & ip-deform (19a)
	ν_{31}	1425	1424	ring str & ip-deform (19b)
	ν_{32}	1353	1340	vinyl CH ip-bend, ring str ((14)
	ν_{33}	1272	1271	ring str (13)
	ν_{34}	1206	1211	vinyl CH ip-bend
	ν_{35}	1108	1107	CH ip-bend (18b)
	ν_{36}	1000	1014	CH ip-bend (18a)
	ν_{37}	794	784	ring ip-deform(12)
	ν_{38}	435	430	skeletal ip-deform

str, stretch; ip, in-plane; op, out-of-plane; deform, deformation.

active in-plane vibrations. The IR bands observed at 3110, 3077, 3024, 1519, 1424, 1340, 1271, 1211, 1107, 1014, 784, and 430 cm^{-1} are assigned to the $\nu_{27}(b_u)$–$\nu_{38}(b_u)$ modes, respectively. The 966-cm^{-1} IR band is assigned to $\nu_{15}(a_u)$, that is the CH out-of-plane wagging of the *trans* vinylene groups. No band due to a *cis* vinylene group has been observed; this is an experimental result. These results indicate that the vinylene groups take the *trans* configuration. The 838-cm^{-1} band is assigned to $\nu_{17}(a_u)$, that is the in-phase CH out-of-plane wagging of *para*-disubstituted benzene rings. The 556-cm^{-1} band is also assigned to an out-of-plane vibration, namely $\nu_{18}(a_u)$.

3 RAMAN SPECTRA OF DOPED POLYMERS

Most pristine conjugated polymers show π–π^* electronic absorptions in the region from the ultraviolet to the visible. Upon doping, new absorption bands associated with the sub-gap bands of carriers appear in the region from the visible to the near-IR. Thus, the structures of doped polymers (carriers generated by doping) can be studied by resonance Raman spectroscopy with a wide range of excitation wavelengths from visible to IR.[43] The longest excitation wavelength used so far is 1320 nm. A positive polaron (charge $+e$, spin 1/2) and a negative polaron (charge $-e$, spin 1/2) correspond to the radical cation and the radical anion of an oligomer, respectively. A positive bipolaron (charge $+2e$, spin 0) and a negative bipolaron (charge $-2e$, spin 0) correspond to the closed-shell dication and the closed-shell dianion of an oligomer, respectively. Thus, marker bands for identifying polarons and bipolarons can be obtained from studies of the radical ions and the divalent ions of oligomers. The studies of charged oligomers are very important.

Before going on to discuss the Raman studies of doped polymers, it is useful to describe the electronic states of charge carriers in conjugated polymers.[21,22,44,45] The schematic electronic structures of carriers are shown in Figure 6. Although the excitonic effect, or electron correlation, plays a significant role in the optical properties of conjugated polymers and oligomers, we will use the one-electron model because of its simplicity. The band structure of a neutral polymer is shown in Figure 6(a). For a polaron or a bipolaron, two localized electronic levels, bonding and antibonding, are formed symmetrically with respect to the gap center at $-\omega_0$ and $+\omega_0$, respectively, as shown in Figure 6(b–e). The positions of the localized electronic levels, i.e., $\pm\omega_0$, depend on the extent of the structural changes associated with the polarons and the bipolarons. When a positive polaron is formed, one electron is removed from the $-\omega_0$ level (Figure 6(b)). Thus a positive polaron has two sub-gap transitions, P_1 and P_2. When a negative polaron is formed, one electron is added to the $+\omega_0$ level (Figure 6(c)). Thus a negative polaron also has two sub-gap transitions, P_1 and P_2. When a positive bipolaron is formed, two electrons are removed from the $-\omega_0$ level (Figure 6(d)). Thus a

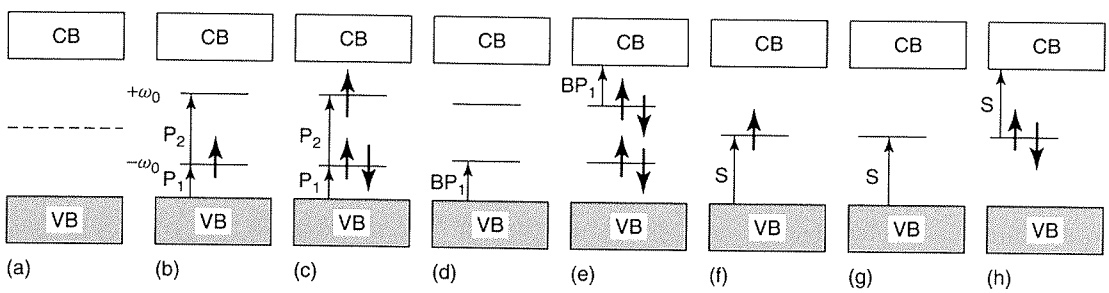

Figure 6. Schematic one-electron electronic structures of elementary excitations: (a) neutral polymer; (b) positive polaron; (c) negative polaron; (d) positive bipolaron; (e) negative bipolaron; (f) neutral soliton; (g) positive soliton; (h) negative soliton.

positive bipolaron has a single sub-gap transition BP_1. When a negative bipolaron is formed, two electrons are added to the $+\omega_0$ level (Figure 6(e)). Thus a negative bipolaron has a single sub-gap transition BP_1. For a positive and a negative soliton, a nonbonding level is formed in the center of the band gap (Figure 6(f) and (h)). Thus, a single sub-gap absorption is expected to be observed at the middle of the band edge of the neutral polymer.

3.1 Doped polyacetylene

Raman spectra of doped polyacetylene have been measured with various excitation wavelengths.[25,46–50] The Raman spectra of *trans*-polyacetylene and heavily Na-doped *trans*-polyacetylene with excitation at 1320 nm,[50] are shown in Figure 7(a) and (b), respectively. Upon Na doping, a broad electronic absorption band appears from the visible to the near-IR, whereas a band peaking at 677 nm (1.83 eV), which is due to neutral *trans*-polyacetylene, disappears completely. Since the excitation wavelength 1320 nm falls inside the doping-induced absorption, the 1320-nm excited Raman spectrum mainly arises from new structures generated by Na doping. It is expected that negative polarons or negative solitons are formed by Na doping. The ν_2 band of *trans*-polyacetylene shows an upward shift from 1469 to 1493 cm^{-1} upon Na doping. The ν_3 band shows a downward shift from 1290 to 1255 cm^{-1}. The ν_4 band also shows an upward shift from 1068 to 1105 cm^{-1}. A broad strong band is observed at 1151 cm^{-1}, which corresponds to the 1172-cm^{-1} band of pristine *trans*-polyacetylene. These spectral changes will be compared with those of model compounds.

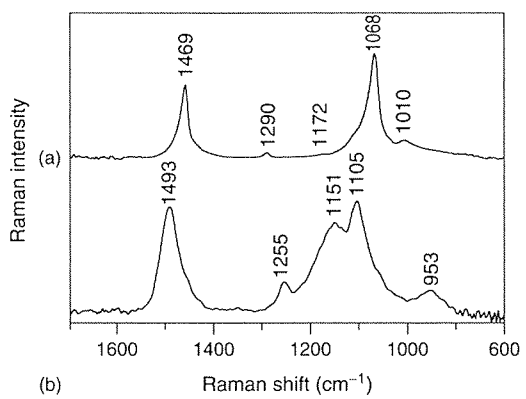

Figure 7. 1320-nm excited Raman spectra of (a) *trans*-polyacetylene and (b) heavily Na-doped *trans*-polyacetylene ($CHNa_{0.14}$). [Reproduced from Yukio Furukawa, 'Vibrational Spectroscopy of Conducting Polymers', in "Handbook of Vibrational Spectroscopy", eds J.M. Chalmers and P.R. Griffiths, John Wiley & Sons, Chichester, 2483–2495, Vol. 4 (2002).]

The Raman spectra of the neutral species, the radical anion, and the dianion of 19, 19′, 20, 20′-tetranor-β,β-carotene, (abbreviated as TNBC, Figure 8) with 11 C=C bonds, are shown in Figure 9.[51] The radical anion corresponds to a negative polaron, whereas the dianion corresponds to two negative solitons. The radical anion of TNBC has an intense absorption at 849 nm (1.46 eV) and a weak band at 1240 nm (1.00 eV), whereas the neutral TNBC has a band peaked at 440 nm (2.82 eV). An intense fluorescence background has prevented us from observing the rigorous resonance Raman spectra of the radical anion using excitation at either 753 nm (1.65 eV) or 781 nm (1.59 eV), inside the 1.46-eV electronic absorption. However, the Raman spectra of the radical anion have been obtained with excitation at both 1064 nm (1.17 eV) and 1320 nm (0.94 eV). The 1551-cm^{-1} and 1496-cm^{-1} bands (C=C stretchings) of the radical anion correspond to the 1597-cm^{-1} and 1522-cm^{-1} bands of neutral

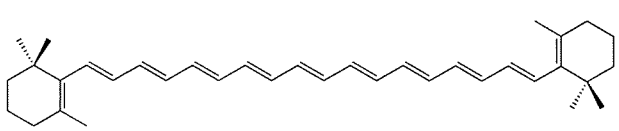

Figure 8. Chemical structure of 19, 19′, 20, 20′-tetranor-β,β-carotene (TNBC).

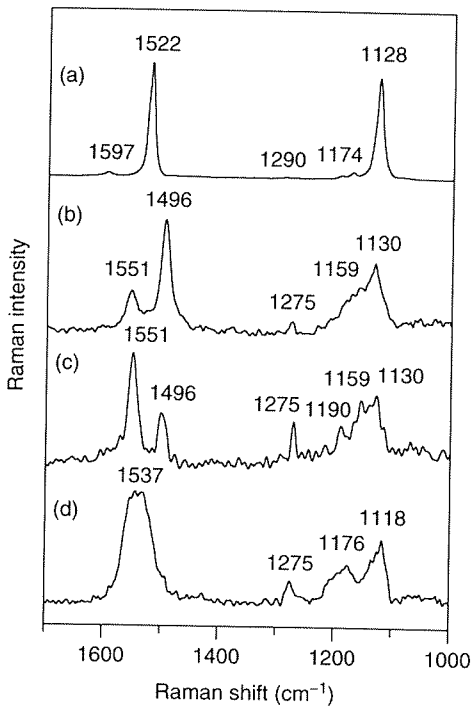

Figure 9. Raman spectra of the various oxidation states of 19, 19′, 20, 20′-tetranor-β,β-carotene: (a) neutral species; (b and c) radical anion; (d) dianion. Excitation wavelengths used in (a), (b), (c), and (d) are 1064, 1064, 1320, and 1064 nm, respectively. (a) Solid; (b), (c), and (d), THF solutions. The bands of THF and background are subtracted in (b), (c), and (d). [Reproduced from Yukio Furukawa, 'Vibrational Spectroscopy of Conducting Polymers', in "Handbook of Vibrational Spectroscopy", eds J.M. Chalmers and P.R. Griffiths, John Wiley & Sons, Chichester, 2483–2495, Vol. 4 (2002).]

TNBC. The lower wavenumber shift of each band reflects a decrease in the C=C bond order. The 1290-cm^{-1} band of TNBC downshifts to 1275 cm^{-1} for the radical anion. The 1128-cm^{-1} band upshifts to 1130 cm^{-1}. This small upshift seems to be the result of strong mixing between the C–C and C=C stretches. The intensity of each of the 1551-, 1275-, 1190-, and 1159-cm^{-1} bands is stronger with excitation at 1320 nm than at 1064 nm.

The dianion of TNBC has an intense absorption at 780 nm (1.59 eV). It was not possible to observe the resonance Raman spectrum of the dianion with excitation at 632.8 or 753 nm, because of the presence of an intense fluorescence background. However, a pre-resonant Raman spectrum of the dianion has been observed with excitation at 1064 nm (Figure 9(d)). The 1537-cm^{-1} broad band of the dianion corresponds to the 1522-cm^{-1} band of neutral TNBC. This 15-cm^{-1} upshift observed for the dianion cannot be explained by a simple consideration of the bond order of the C=C bonds. This upshift may arise from large structural changes on going from the neutral TNBC to the anion. According to *ab initio* molecular orbital calculations of 1,3,5,7,9-decapentaene,[52] bond alternation is reversed in the middle of the chain. The 1275-cm^{-1} band of the dianion corresponds to the 1290-cm^{-1} band of the neutral species. The low wavenumber position of the ν_3 band is a marker for negatively charged polyenes. The 1118-cm^{-1} band of the dianion corresponds to the 1128-cm^{-1} band of the neutral species.

It seems that the spectral changes observed for *trans*-polyacetylene upon Na doping are similar to those observed for TNBC on going from the neutral species to the dianion (two negative solitons). However, further experimental and theoretical studies on the charged species of polyenes are required for a complete analysis of the Raman spectra of Na-doped *trans*-polyacetylene.

3.2 Doped polythiophene

The as-polymerized BF_4^--doped polythiophene prepared by an electrochemical method has two broad absorption bands peaked at 738 and 1700 nm (1.68 and 0.73 eV).[53] In a non-degenerate conjugated polymer such as polythiophene, polarons or bipolarons are expected to be formed by doping. The two observed bands are attributable to positive polarons, because a polaron gives rise to the two sub-gap electronic absorption bands, whereas a positive bipolaron gives rise to a single band. The 1064-nm excited Raman spectra of a pristine polythiophene film and an as-polymerized BF_4^--doped polythiophene film are shown in Figure 10(a) and (b),

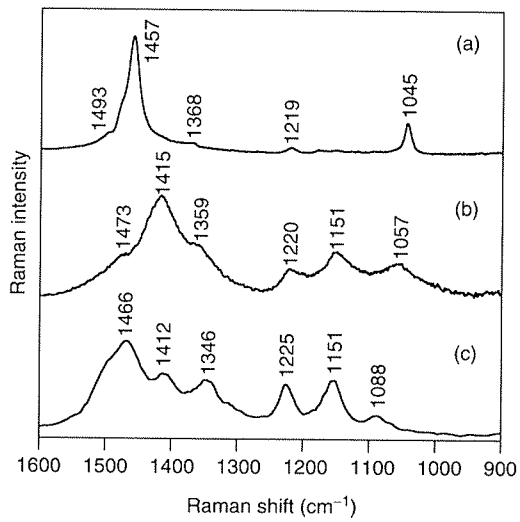

Figure 10. 1064-nm excited FT-Raman spectra of (a) a pristine polythiophene film, (b) a polythiophene film doped with BF_4^-, and (c) a polythiophene film doped with $FeCl_3$ vapor.

respectively.[53] The spectra taken with excitation at 633 and 753 nm are essentially the same as that at 1064 nm. The observed spectra of the BF_4^--doped polythiophene are different from that of the pristine polymer film. The observed spectra are probably attributable to the positive polarons (carriers) generated by doping.

A polythiophene film doped with the vapor of $FeCl_3$ shows a single broad absorption band around 1409 nm (0.88 eV) (D. Okamura, H. Hamaki, S. Tagami, and Y. Furukawa, private communications). This band can be attributed to positive bipolarons, because a bipolaron give rise to a single sub-gap electronic absorption band. The 1064-nm excited Raman spectrum of the vapor-phase $FeCl_3$-doped polythiophene film is shown in Figure 10(c). The spectrum taken at 753 nm is essentially the same as that at 1064 nm. These spectra are quite different from those of the pristine and the BF_4^--doped polythiophene films. The observed spectra of the vapor-phase $FeCl_3$-doped polythiophene film are probably attributed to positive bipolarons.

α-Sexithiophene (Figure 11) is a linear conjugated oligomer having six thiophene rings. The

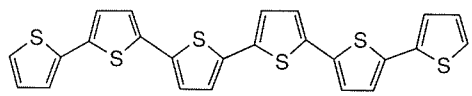

Figure 11. Chemical structure of α-sexithiophene.

radical cation and the dication of α-sexithiophene correspond to a positive polaron and a positive bipolaron, respectively. Thus, the Raman spectra of the radical cation and the dication are useful for determining the types of carriers generated by doping. The Raman spectra of the neutral species, the radical cation, and the dication of α-sexithiophene are shown in Figure 12.[53] The 1064-nm excited Raman spectrum of BF_4^--doped polythiophene (Figure 10(b)) is quite similar to that of the radical cation (Figure 12(b)), but is different from that of the dication (Figure 12(c)). This indicates that positive polarons are generated in the BF_4^--doped polythiophene film, which is consistent with the conclusion drawn from electronic absorption spectroscopy. The strongest band at 1440 cm^{-1} is probably assigned to the mixture of the C=C and C–C stretchings.[54–56] We can find some common features in the spectra of the dication of α-sexithiophene and vapor-phase $FeCl_3$-doped polythiophene, except for the

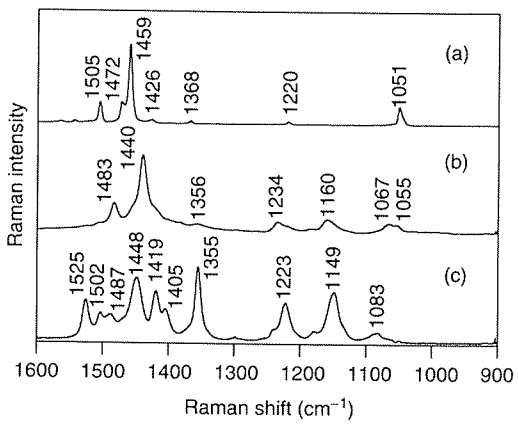

Figure 12. Raman spectra of the various oxidation states of α-sexithiophene: (a) neutral species; (b) radical cation; (c) dication. Excitation wavelengths used in (a), (b), and (c) are 1064, 781, and 781 nm, respectively. (a) Solid; (b) CH_2Cl_2 solution; (c) CD_2Cl_2 solution. The bands of the solvents and backgrounds are subtracted in (b) and (c).

range between 1540 and 1440 cm^{-1}. In the spectrum of vapor-phase $FeCl_3$-doped polythiophene a strong band is observed at 1466 cm^{-1}, whereas four bands are observed at 1525, 1502, 1487, and 1448 cm^{-1} in the spectrum of the dication of α-sexithiophene.

Positive polarons are formed in the as-polymerized BF_4^--doped polythiophene. On the other hand, positive bipolarons are formed in vapor-phase $FeCl_3$-doped polythiophene from light to heavy doping levels. The positive bipolarons are separated into positive polarons upon heating and exposure to air (D. Okamura, H. Hamaki, S. Tagami, and Y. Furukawa, private communications). When a polythiophene film is doped with a dichloromethane solution of $FeCl_3$, different results have been obtained; positive polarons are formed at light and medium doping levels, and positive bipolarons at a heavy doping level (D. Okamura, H. Hamaki, S. Tagami, and Y. Furukawa, private communications).

3.3 Doped poly(p-phenylenevinylene)

Upon sulfuric-acid (H_2SO_4) doping, the electronic absorption band of the neutral polymer disappears and new absorption bands appear at 551 and 1240 nm (2.25 and 1.00 eV).[57] These two absorptions are due to positive polarons generated by sulfuric-acid doping. The Raman spectra of a H_2SO_4-doped poly(*p*-phenylenevinylene) film with excitation at 441.6, 514.5, 632.8, 711.0, 740.0, and 1064 nm, which fall inside the broad absorption observed at 2.25 eV, have been reported.[57] The observed spectra are similar to each other. These spectra are essentially the same as the Raman spectrum of the radical cation of an oligomer having two vinylene groups and three benzene rings. The radical cation corresponds to a positive polaron. Thus, these spectra arise from positive polarons generated by H_2SO_4 doping. The 1064-nm excited spectrum is different from those obtained with other wavelengths. It has been concluded that this spectrum is contributed to by the inter-chain polaron dimers, on the basis of the Raman spectra of the dimer of the radical cations of the model oligomer.[58]

A single electronic absorption band appears at 800 nm (1.55 eV) upon Na doping,[20] which is in contrast to the result of H_2SO_4 doping. It is commonly believed that this band is attributable to bipolarons, because a bipolaron gives rise to a single sub-gap absorption band. On the other hand, different results have been obtained from a Raman study.[59] The Raman spectra of a Na-doped poly(*p*-phenylenevinylene) film with excitation at 488.0, 514.5, 632.8, 711.0, 740.0, and 1064 nm have been reported.[59] The observed spectra strongly depend on excitation wavelength. These spectra have been analyzed on the basis of the Raman spectra of the radical anions and the dianions of three oligomers. As a result, the observed Raman spectra of Na-doped poly(*p*-phenylenevinylene) have been explained by the coexistence of polarons and bipolarons having various localization lengths. Since each species has its own electronic absorption, the Raman bands due to the species are resonantly enhanced by choosing the excitation wavelength within the broad doping-induced absorption band. The major species generated by Na doping is a negative bipolaron, because the electronic absorption shows the single band at 1.55 eV.

4 DOPING-INDUCED IR ABSORPTION

The charge carriers in conjugated polymers can be generated by chemical doping. The formation of carriers such as polarons, bipolarons, and charged solitons are associated with structural changes and localized vibrational modes, as well as localized electronic states within the band gap. Doping-induced IR active vibrational (IRAV) modes have been observed in the IR region.[60] The iodine-doping-induced IR absorption spectrum of *trans*-polyacetylene is shown in Figure 13(a). The iodine- and vapor-phase $FeCl_3$-doping-induced IR spectra of polythiophene are shown in Figure 13(b) and (c), respectively. The

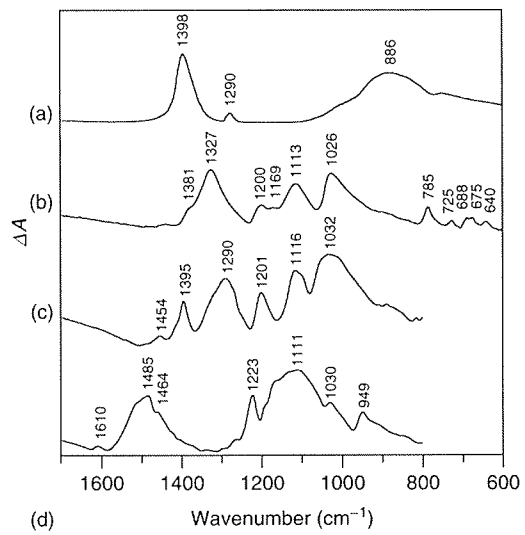

Figure 13. IR absorption spectra of (a) iodine-doped *trans*-polyacetylene, (b) iodine-doped polythiophene; (c) vapor-phase $FeCl_3$-doped polythiophene; (d) iodine-doped MEH-PPV. [Reproduced from Yukio Furukawa, 'Vibrational Spectroscopy of Conducting Polymers', in "Handbook of Vibrational Spectroscopy", eds J.M. Chalmers and P.R. Griffiths, John Wiley & Sons, Chichester, 2483–2495, Vol. 4 (2002).]

iodine-doping-induced IR spectrum of poly(2-methoxy-5-(2′-ethylhexyloxy)-*p*- phenylenevinylene) (MEH-PPV) is shown in Figure 13(d). The absorption coefficients of the doping-induced IR bands are far larger than those of pristine polymers. The generated charged species give rise to very intense IR bands. Thus, even if the concentration of carriers is very low, the carriers can be detected by IR spectroscopy. The doping-induced IR bands and the Raman spectra of pristine polymers have been explained successfully in terms of the ECC theory proposed by Zerbi *et al.*[17,19] In their model, charge oscillation along the polymer chain induces strong IR intensities. The vibrational modes corresponding to the totally symmetric modes, which induce oscillation in bond alternation for a neutral polymer, are intense in the observed IR spectra due to carriers generated by chemical doping. Thus, the doping-induced IR bands correspond to the totally symmetric Raman bands of the pristine polymer. However, the number of doping-induced IR bands is in general larger than that of the totally symmetric modes of the pristine polymer. For example, in the IR spectrum of iodine-doped polythiophene 11 doping-induced bands are observed, although there are only $7a_g$ modes. It should be noted that the ECC theory is only an approximation. It is expected that normal coordinate calculations based on *ab initio* molecular orbital methods, and density functional theory for the charged oligomers, will be useful in analyzing doping-induced IR spectra.

It has been demonstrated[21–23] that the types of carriers can be identified by sub-gap electronic transitions appearing in the region from the visible to the IR. In lightly iodine-doped polythiophene, two sub-gap absorption bands are observed. These two bands are attributable to positive polarons. Therefore, the doping-induced IR bands of iodine-doped polythiophene (Figure 13(b)) are also ascribed to positive polarons. On the other hand, in the vapor-phase $FeCl_3$-doped polythiophene, a single sub-gap absorption is observed. Since the absorption is attributed to positive bipolarons, the doping-induced IR bands (Figure 13(c)) are also ascribed to positive bipolarons. The infrared spectrum of positive polarons is markedly different from that of positive bipolarons in the wavenumber range between 1450 and 1250 cm^{-1}. The polarons give rise to the 1327-cm^{-1} band with the 1381-cm^{-1} shoulder, whereas the bipolarons yield the 1395-cm^{-1} and 1290-cm^{-1} bands. Two sub-gap absorption bands are observed for iodine-doped MEH-PPV, which are attributed to positive polarons. Thus, the observed IR spectrum of iodine-doped MEH-PPV (Figure 13(d)) is also ascribed to positive polarons. In the case of *trans*-polyacetylene having a degenerate ground state, doping-induced IR absorption spectra are assigned to charged solitons.[60–62]

5 PHOTO-INDUCED IR ABSORPTION

The charge carriers in conjugated polymers can be generated by light irradiation as well as chemical

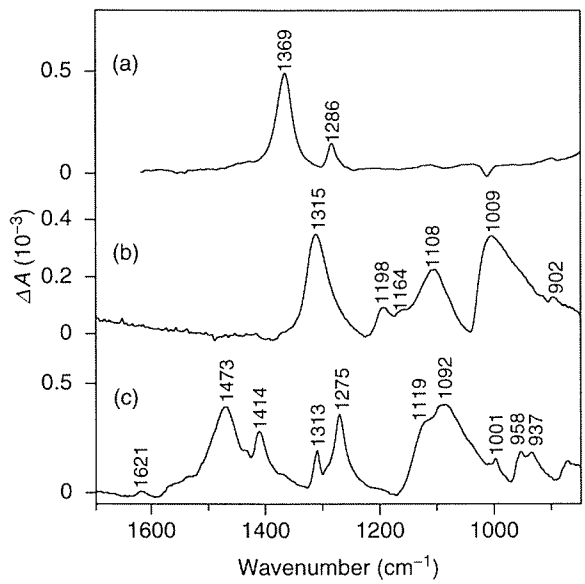

Figure 14. Photo-induced IR absorption spectra of conjugated polymers: (a) *trans*-polyacetylene; (b) polythiophene; (c) poly(*p*-phenylenevinylene). Temperature is 78 K. [Reproduced from Yukio Furukawa, 'Vibrational Spectroscopy of Conducting Polymers', in "Handbook of Vibrational Spectroscopy", eds J.M. Chalmers and P.R. Griffiths, John Wiley & Sons, Chichester, 2483–2495, Vol. 4 (2002).]

doping. Photo-induced IR difference absorptions are therefore observed.[61–63] Photo-induced IR absorption spectra of *trans*-polyacetylene, polythiophene, and poly(*p*-phenylenevinylene) are shown in Figure 14(a–c), respectively. Photo-induced IR spectra of polythiophene and poly(*p*-phenylenevinylene) are also ascribed to polarons generated by light irradiation, because two photo-induced electronic absorptions are observed. The decay mechanism of photo-generated carriers on the micro- to millisecond timescale has been studied by means of a phase–modulation technique.[64,65] The observed results have been explained on the basis of second-order kinetics involving a neutralization-recombination process between positive and negative polarons. The mechanism of carrier generation induced by light irradiation has been studied by picosecond time-resolved IR spectroscopy.[66,67]. Moses *et al.*[66] have concluded that carriers are photoexcited directly, and are not generated via excitons. However, carrier generation via excitons has been proposed by Köhler *et al.*[68]

Conjugated polymer/C_{60} composites are promising candidates for photovoltaic cells and solar cells, because the addition of C_{60} into a conjugated polymer enhances the efficiency of charge

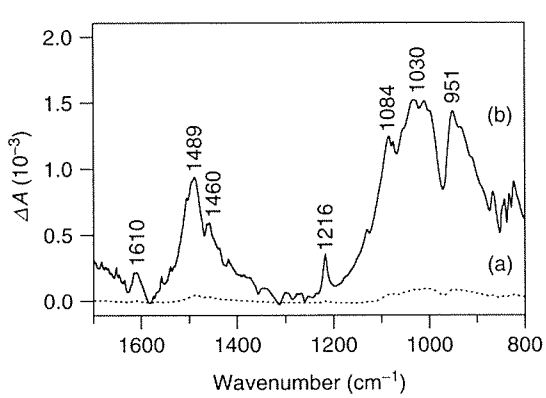

Figure 15. Photo-induced IR absorption spectra of (a) DOO-PPV and (b) DOO-PPV/C_{60} composite. Temperature is 78 K. [Reproduced from Yukio Furukawa, 'Vibrational Spectroscopy of Conducting Polymers', in "Handbook of Vibrational Spectroscopy", eds J.M. Chalmers and P.R. Griffiths, John Wiley & Sons, Chichester, 2483–2495, Vol. 4 (2002).]

separation upon light irradiation.[69] In a composite of a conjugated polymer and C_{60}, electrons are transferred from photo-generated excitons in the conjugated polymer to C_{60}.[69] Ultrafast spectroscopy has shown that the charge separation occurs within a few hundred femtoseconds, with a very slow back-transfer.[70] The photo-induced IR absorption spectra of poly(2,5-dioctyloxy-*p*-phenylenevinylene) (DOO-PPV) and DOO-PPV/C_{60} composite measured at 77 K are shown in Figure 15(a) and (b), respectively (K. Kudo and Y.Y. Furukawa, private communications). Photo-induced spectra are attributed to polarons generated by light irradiation. The intensities of the bands due to polarons are enhanced more than 10 times by the addition of C_{60}.

6 RAMAN SPECTROSCOPY OF POLYMER LEDS

Conjugated polymers such as poly(*p*-phenylene-vinylene) derivatives, polyfluorene derivatives, etc. are used as active materials in polymer LEDs.[8,9] The schematic structure of a double-layer polymer LED is shown in Figure 16. In polymer LEDs, it is considered that positive carriers are injected from an indium-tin-oxide (ITO) anode into the polymer layer, and negative carriers from the cathode, by the application of a voltage. Light emission results from the radiative decay of the singlet excitons formed by the recombination of the

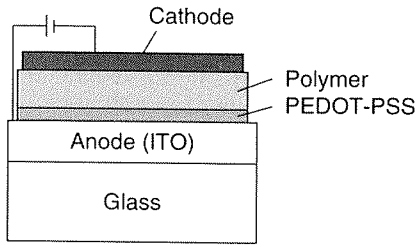

Figure 16. Schematic structure of a double-layer polymer LED.

injected positive and negative carriers. The use of poly(3,4-ethylenedioxythiophene)-poly(4-styrenesulfonate) (PEDOT-PSS, Figure 17(a)) as a hole-injection layer between the ITO anode and an active polymer layer improves device efficiency, brightness, and lifetime considerably. In PEDOT-PSS, PEDOT chains are doped (oxidized), and counter anions are $-SO_3^-$ groups of PSS. Commercialization of polymer LEDs will require longer device lifetimes. Micro-Raman spectroscopy is useful for developing a better understanding of the degradation mechanism in polymer LEDs.[71–73] Sakamoto *et al.*[73] have reported the structural changes of PEDOT chains upon operation in a double-layer polymer LED fabricated with poly(2,7-(9,9-dioctylfluorene)-*alt*-benzothiadiazole) (F8BT, Figure 17(b)) blended with poly(9,9-dioctylfluorene) (PF8, Figure 17(c)) as an emissive layer. The 633-nm excited Raman spectra of the polymer LED with the ITO/PEDOT-PSS/F8BT-PF8/Li-Al structure are shown in Figure 18. The spectrum of the

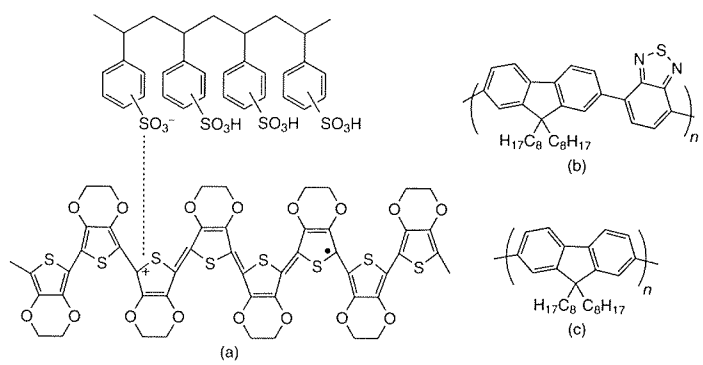

Figure 17. Chemical structures of (a) PEDOT-PSS, (b) F8BT, and (c) PF8.

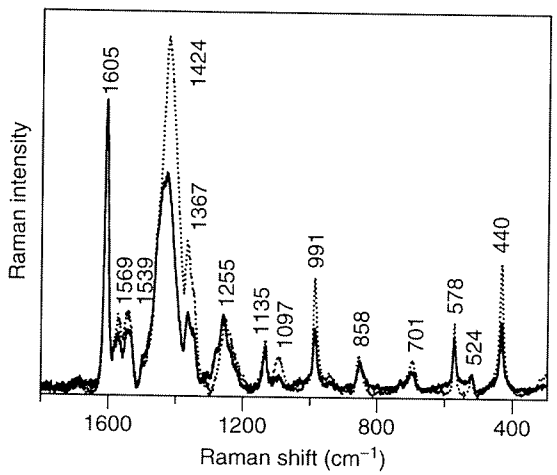

Figure 18. Raman spectra of a polymer LED with the ITO/PEDOT-PSS/F8BT-PF8/Li-Al structure before (solid line) and after (dotted line) the operation. Excitation wavelength was 633 nm.

as-prepared LED is shown as the solid line; the spectrum of the LED operated at 10 V for 30 min as the dotted line. In the spectrum of the initial LED, the bands observed at 1605, 1135, and 858 cm^{-1} have been attributed to PF8; the bands observed at 1569, 1539, 1424, 1367, 1255, 991, 701, 578, 524, and 440 cm^{-1} to PEDOT. No bands of F8BT and PSS are observed. The relative intensities of the bands due to PEDOT, PSS, PF8, and F8BT depend on the amount of each polymer, the resonance Raman effect, and the electric field in the polymer layer. Upon the operation, the bands at 1569, 1539, 1424, 1367, 1097, 991, 854, 701, 578, and 440 cm^{-1} increase significantly in intensity. These bands are attributed to PEDOT. Upon the electrochemical reduction of an as-prepared PEDOT-PSS film, a new absorption appears at about 630 nm, which is assigned to the $\pi - \pi^*$ absorption of neutral parts of PEDOT chains. Upon electrochemical reduction, the intensities of the Raman bands due to PEDOT increase, which is consistent with the concomitant appearance of the 630-nm absorption band. On the basis of these results, it can be concluded that the observed intensity increases of bands due to PEDOT in the polymer LED upon the operation arise from the reduction (dedoping) of the PEDOT chains. It causes changes in the electronic states of the PEDOT chains and the efficiency of hole injection. Thus, the polymer LED may be degraded.

It has been shown that Raman spectroscopy gives us the information about the crystalline/amorphous states of hole-transport materials in organic LEDs.[74] IR spectroscopy is useful for detecting carriers injected into the polymer layer in LEDs.[75,76]

7 IR SPECTROSCOPY IN POLYMER FETS

Conjugated polymers such as regioregular poly(3-alkylthiophene)s, poly(*p*-phenylenevinylene) derivatives, polydiacetylenes, etc. (see Figure 1) have been incorporated as active semiconductors in organic FETs.[2,5,6] A polymer FET is composed of a thin polymer semiconductor layer, an insulator layer, and three electrodes: source, drain, and gate. Two common device configurations used in polymer FETs are shown in Figure 19(a) and (b), which are called the top-contact and the bottom-contact configurations, respectively. The polymer FET operates like a capacitor.[77] When a voltage is applied between the source and the gate electrodes, a charge is injected from the source electrode into the polymer

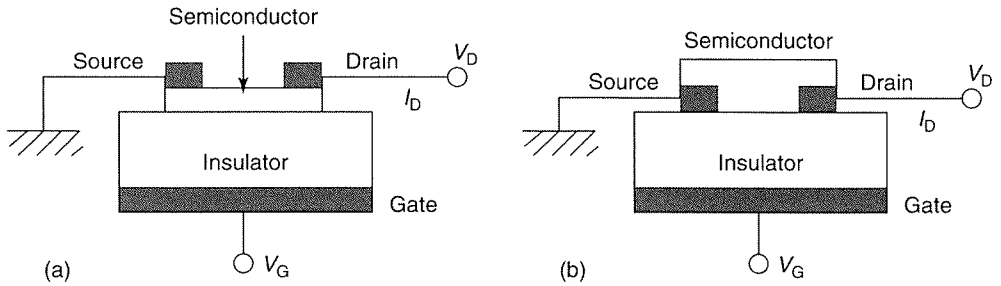

Figure 19. Schematic device structures of (a) top- and (b) bottom-contact FETs.

film. Then, the injected charge is accumulated at the insulator–semiconductor interface. This charge forms a conducting region, which is called the channel, between the source and the drain electrodes. Accordingly, a current flows between the source and the drain electrodes through the conducting channel. When a voltage is not applied between the source and the gate electrodes, the conducting channel is not formed. Thus, a current does not flow between the source and the drain electrodes. The characteristics of the FET depend on the density, the distribution, and the mobility of carriers. However, the behavior of carriers has not yet been fully elucidated. It has been demonstrated that IR spectroscopy is very useful for studying carriers in polymer FETs, because carriers give rise to intense IRAV bands.[78–82]

Voltage-induced IR absorption from a polymer FET can be obtained by difference IR spectroscopy. The gate-voltage-induced IR absorption has been measured on a Fourier transform infrared (FT-IR) spectrometer by using a polymer FET with interdigital source and drain electrodes (Figure 20).[78–82] The incident IR beam passes through the region between the interdigital source and drain electrodes. The IR spectrum of a thin film of MEH-PPV is shown in Figure 21(a). The gate-voltage-induced IR absorption spectrum from the FET with the *n*-Si(gate)/SiO_2/MEH-PPV/Au(source & drain) structure is shown in Figure 21(b). The source and the drain electrodes are connected with each other. The spectrum is the difference between spectra acquired at gate voltages of −40 and 5 V. The observed positive bands in Figure 21(b) have been attributed to

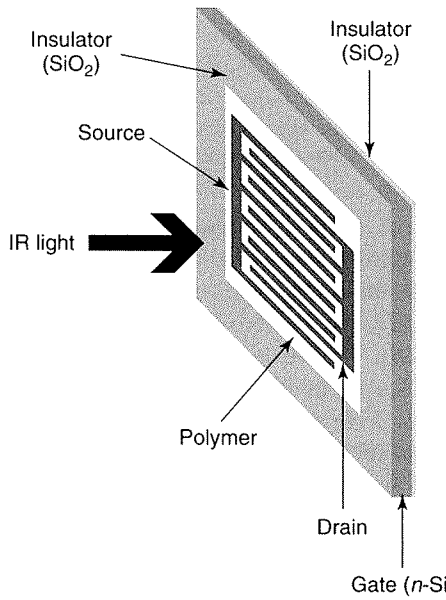

Figure 20. Schematic picture of voltage-induced IR absorption measurements.

positive carriers (positive polarons) injected into the MEH-PPV film. The positive charges injected into the MEH-PPV film forms positive polarons, which accumulate at the MEH-PPV/SiO_2 interface in the channel. The cross section of the 1510-cm^{-1} IR band has been measured as 7.7×10^{-17} cm^2 for the MEH-PPV films doped electrochemically with ClO_4^-. Figure 22 shows the change in absorbance of the 1510-cm^{-1} band as a function of the gate voltage V_G for the top- and bottom-contact FETs. It is believed that carriers generated by the field effect exist as a very thin sheet at the polymer–insulator interface. Thus,

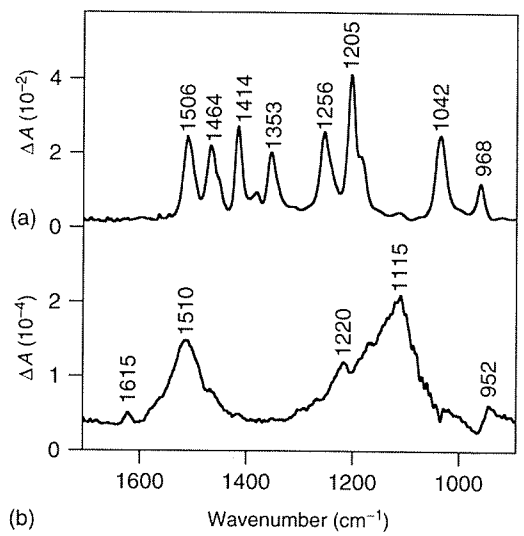

Figure 21. (a) IR spectrum of an MEH-PPV film and (b) gate-voltage-induced IR absorption spectrum from the FET with the *n*-Si(gate)/SiO_2/MEH-PPV/Au(source & drain) structure. The source and the drain electrodes are connected with each other. The spectrum is the difference between the gate voltages of −40 and 5 V.

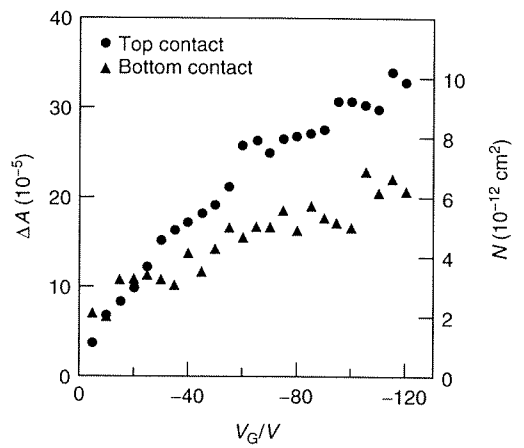

Figure 22. Relation between the peak intensity of the 1500-cm^{-1} band, the carrier sheet density (N), and the gate voltage (V_G). The ΔA means the difference between V_G ($V_G < 0$) and $-V_G$. The source and the drain electrodes are connected with each other.

decadic absorbance can be expressed in terms of a charge per unit area, i.e., the carrier sheet density N [cm^{-2}], as follows:

$$A = (\log e)\sigma N \approx 0.4343\sigma N \qquad (1)$$

where σ [cm^2] means the cross section of a band due to carriers. The carrier sheet density can be obtained from Equation (1) by using the value of σ. Since the injected carriers are probably not distributed uniformly in the channel, one can obtain average carrier sheet densities. Figure 22 shows that N is not proportional to V_G for both of the top- and bottom-contact configurations. The carrier sheet density in the top-contact device is larger than that in the bottom-contact device at a value of V_G in the range below −20 V. The induced carrier sheet density depends on the geometrical structure of the FETs. The maximum carrier sheet density has been determined to be about 10^{13} cm^{-2}.

8 CONCLUDING REMARKS

It has been demonstrated that IR and Raman spectroscopy are powerful tools for studying the structures of doped and pristine conjugated polymers. The charge carriers such as charged solitons, polarons, and bipolarons can be identified by IR and Raman spectroscopy. In particular, IR spectroscopy is very useful for detecting the photogenerated and injected carriers in polymer optoelectronic devices, because the carriers give rise to very intense IR bands. *In situ* IR and Raman spectroscopy will give us information about polymer structures and carriers in light-emitting diodes, field-effect transistors, and solar cells fabricated with conjugated polymers.

ABBREVIATIONS AND ACRONYMS

DOO-PPV	Dioctyloxy-*p*-phenylenevinylene
ECC	Effective Conjugation Coordinate
FETs	Field-Effect Transistors
FT-IR	Fourier Transform Infrared
IR	Infrared
IRAV	Ir Active Vibrational
ITO	Indium-Tin-Oxide

LEDs	Light-Emitting Diodes
MEH-PPV	Methoxy-5-(2′-Ethylhexyloxy)-*p*-Phenylenevinylene)
PEDOT-PSS	Poly(3,4-ethylenedioxythiophene)-Poly(4-Styrenesulfonate)

REFERENCES

1. H. Kiess (ed), 'Conjugated Conducting Polymers', Springer-Verlag, Berlin (1992).
2. N.C. Greenham and R.H. Friend, *Solid State Phys.*, **49**, 1–149 (1995).
3. T.A. Skotheim, R.L. Elsenbaumer and J.R. Reynolds (eds), 'Handbook of Conducting Polymers', Marcel Dekker, New York (1997).
4. N.S. Sariciftci (ed), 'Primary Photoexcitations in Conjugated Polymers: Molecular Exciton Versus Semiconductor Band Model', World Scientific, Singapore (1997).
5. A. Tsumura, H. Koezuka and T. Ando, *Appl. Phys. Lett.*, **49**, 1210–1212 (1986).
6. J.H. Burroughes, C.A. Jones and R.H. Friend, *Nature*, **335**, 137–141 (1988).
7. G. Yu, J. Gao, J.C. Hummelen, F. Wudl and A.J. Heeger, *Science*, **270**, 1789–1791 (1995).
8. J.H. Burroughes, D.D.C. Bradley, A.R. Brown, R.N. Marks, K. Mackay, R.H. Friend, P.L. Burns and A.B. Holmes, *Nature*, **347**, 539–541 (1990).
9. R.H. Friend, R.W. Gymer, A.B. Holmes, J.H. Burroughes, R.N. Marks, C. Taliani, D.D.C. Bradley, D.A. Dos Santos, J.L. Brédas, M. Lögdlund and W.R. Salaneck, *Nature*, **397**, 121–128 (1999).
10. W.P. Su, J.R. Schrieffer and A.J. Heeger, *Phys. Rev., B*, **22**, 2099–2111 (1980).
11. W.P. Su and J.R. Schrieffer, *Proc. Natl. Acad. Sci. U.S.A.*, **77**, 5626–5629 (1980).
12. S.A. Brazovskiĭ and N.N. Kirova, *Sov. Phys. JETP Lett.*, **33**, 4–8 (1981).
13. A.R. Bishop, D.K. Campbell and K. Fesser, *Mol. Cryst. Liq. Cryst.*, **77**, 253–264 (1981).
14. J.L. Brédas, R.R. Chance and R. Silbey, *Mol. Cryst. Liq. Cryst.*, **77**, 319–332 (1981).
15. H. Kuzmany, *Makromol. Chem., Macromol. Symp.*, **37**, 81–97 (1990).
16. I. Harada and Y. Furukawa, 'Vibrational Spectra and Structure of Conjugated and Conducting Polymers', in "Vibrational Spectra and Structure", ed J.R. Durig, Elsevier, Amsterdam, Vol. 19 (1991).
17. M. Gussoni, C. Castiglioni and G. Zerbi, 'Vibrational Spectroscopy of Polyconjugated Materials: Polyacetylene and Polyenes', in "Spectroscopy of Advanced Materials", eds R.J.H. Clark and R.E. Hester, John Wiley & Sons, Chichester (1991).
18. A.J. Epstein, R.P. McCall, J.M. Ginder and A.G. MacDiarmid, 'Spectroscopy and Photoexcitation Spectroscopy of Polyaniline: A Model System for New Phenomena', in "Spectroscopy of Advanced Materials", eds R.J.H. Clark and R.E. Hester, John Wiley & Sons, Chichester (1991).
19. G. Zerbi, M. Gussoni, and C. Castiglioni, 'Vibrational Spectroscopy of Polyconjugated Aromatic Materials with Electrical and Nonlinear Optical Properties. A Guided Tour', in "Conjugated Polymers", eds J.L. Brédas and R. Silbey, Kluwer Academic Publishers, Dordrecht (1991).
20. Y. Furukawa, A. Sakamoto and M. Tasumi, *Macromol. Symp.*, **101**, 95–102 (1996).
21. Y. Furukawa, *J. Phys. Chem.*, **100**, 15644–15653 (1996).
22. Y. Furukawa and M. Tasumi, 'Vibrational Spectroscopy of Intact and Doped Conjugated Polymers and their Models', in "Modern Polymer Spectroscopy", ed G. Zerbi, Wiley-VCH, Weinheim (1991).
23. Y. Furukawa, 'Vibrational Spectroscopy of Conjugated Polymers', in "Handbook of Vibrational Spectroscopy", eds J.M. Chalmers and P.R. Griffiths, John Wiley & Sons, Chichester, Vol. 4 (2002).
24. H. Shirakawa and S. Ikeda, *Polym. J.*, **2**, 231–244 (1971).
25. H. Kuzmany, *Phys. Stat. Sol. (B)*, **97**, 521–531 (1980).
26. G. Zannoni and G. Zerbi, *J. Mol. Struct.*, **100**, 485–504 (1983).
27. D. Jumeau, S. Lefrant, E. Faulques and J.P. Buisson, *J. Phys.*, **44**, 819–825 (1983).
28. H. Takeuchi, T. Arakawa, Y. Furukawa, I. Harada and H. Shirakawa, *J. Mol. Struct.*, **158**, 179–193 (1987).
29. S. Hirata, H. Torii and M. Tasumi, *J. Chem. Phys.*, **103**, 8964–8979 (1995).

30. C. Castiglioni, J.T.L. Navarrete, G. Zerbi and M. Gussoni, *Solid State Commun.*, **65**, 625–630 (1988).
31. B. Horovitz, *Solid State Commun.*, **41**, 729–734 (1982).
32. E. Ehrenfreund, Z. Vardeny, O. Brafman and B. Horovitz, *Phys. Rev., B*, **36**, 1535–1553 (1987).
33. K. Akagi, G. Piao, S. Kaneko, K. Sakamaki, H. Shirakawa and M. Kyotani, *Science*, **282**, 1683–1686 (1998).
34. G. Poussigue and C. Benoit, *J. Phys.: Condens. Matter*, **1**, 9547–9560 (1989).
35. E. Faulques, W. Wallnöfer and H. Kuzmany, *J. Chem. Phys.*, **90**, 7585–7593 (1989).
36. C.X. Cui, M. Kertesz and H. Eckhardt, *Synth. Met.*, **43**, 3491–3496 (1991).
37. J.T.L. Navarrete and G. Zerbi, *J. Chem. Phys.*, **94**, 957–964 (1991).
38. M. Kofranek, T. Kovár, H. Lischka and A. Karpfen, *J. Mol. Struct. (Theochem)*, **259**, 181–198 (1992).
39. G. Louarn, J.-Y. Mevellec, J.P. Buisson and S. Lefrant, *Synth. Met.*, **55**, 587–592 (1993).
40. B. Tian, G. Zerbi and K. Müllen, *J. Chem. Phys.*, **95**, 3198–3207 (1991).
41. I. Orion, J.P. Buisson and S. Lefrant, *Phys. Rev., B*, **57**, 7050–7065 (1998).
42. K. Honda, Y. Furukawa and H. Nishide, *Vib. Spectrosc.*, **40**, 149–154 (2006).
43. Y. Furukawa, A. Sakamoto, H. Ohta and M. Tasumi, *Synth. Met.*, **49**, 335–340 (1992).
44. Y. Furukawa, *Synth. Met.*, **69**, 629–632 (1995).
45. Y. Furukawa, 'Do Bipolarons Exist in Doped or Photoirradiated Conjugated Polymers?–An Analysis Based on the Studies of Model Compounds', in "Primary Photoexcitations in Conjugated Polymers: Molecular Exciton versus Semiconductor Band Model", ed N.S. Sariciftci, World Scientific, Singapore (1997).
46. I. Harada, Y. Furukawa, M. Tasumi and H. Shirakawa, *J. Chem. Phys.*, **73**, 4746–4757 (1980).
47. J. Tanaka, Y. Saito, M. Shimizu, C. Tanaka and M. Tanaka, *Bull. Chem. Soc. Jpn.*, **60**, 1595–1605 (1987).
48. Y. Furukawa, H. Ohta, A. Sakamoto and M. Tasumi, *Spectrochim. Acta*, **47A**, 1367–1373 (1991).
49. S. Lefrant, E. Mulazzi and C. Mathis, *Phys. Rev., B*, **49**, 13400–13407 (1994).
50. J.-Y. Kim, S. Ando, A. Sakamoto, Y. Furukawa and M.Tasumi, *Synth. Met.*, **89**, 149–152 (1997).
51. J.-Y. Kim, Y. Furukawa and M. Tasumi, *Chem. Phys. Lett.*, **276**, 418–422 (1997).
52. Y. Kawashima, K. Nakayama, H. Nakano and K. Hirao, *Chem. Phys. Lett.*, **267**, 82–90 (1997).
53. N. Yokonuma, Y. Furukawa, M. Tasumi, M. Kuroda and J. Nakayama, *Chem. Phys. Lett.*, **255**, 431–436 (1996).
54. Ch. Ehrendorfer and A. Karpfen, *Vib. Spectrosc.*, **8**, 293–303 (1995).
55. Ch. Ehrendorfer and A. Karpfen, *J. Phys. Chem.*, **99**, 5341–5353 (1995).
56. J. Casado, V. Hernández, S. Hotta and J.T.L. Navarrete, *J. Chem. Phys.*, **109**, 10419–10429 (1998).
57. A. Sakamoto, Y. Furukawa and M. Tasumi, *J. Phys. Chem.*, **98**, 4635–4640 (1994).
58. A. Sakamoto, Y. Furukawa and M. Tasumi, *J. Phys. Chem. B*, **101**, 1726–1732 (1997).
59. A. Sakamoto, Y. Furukawa and M. Tasumi, *J. Phys. Chem.*, **96**, 3870–3874 (1992).
60. C.R. Fincher, Jr, M. Ozaki, A.J. Heeger and A.G. MacDiarmid. *Phys. Rev., B*, **19**, 4140–4148 (1979).
61. Z. Vardeny, J. Orenstein and G.L. Baker, *Phys. Rev. Lett.*, **50**, 2032–2035 (1983).
62. G.B. Blanchet, C.R. Fincher, T.C. Chung and A.J. Heeger, *Phys. Rev. Lett.*, **50**, 1938–1941 (1983).
63. Y.-H. Cha, Y. Furukawa, M. Tasumi, T. Noguchi and T. Ohnishi, *Chem. Phys. Lett.*, **273**, 159–163 (1997).
64. Y. Furukawa, *Appl. Spectrosc.*, **47**, 1405–1410 (1993).
65. Y. Furukawa, Y.-H. Cha, T. Noguchi, T. Ohnishi and M. Tasumi, *J. Mol. Struct.*, **521**, 211–220 (2000).
66. D. Moses, A. Dogariu and A.J. Heeger, *Chem. Phys. Lett.*, **316**, 356–360 (2000).
67. A. Sakamoto, O. Nakamura, G. Yoshimoto and M. Tasumi, *J. Phys. Chem. A*, **104**, 4198–4202 (2000).
68. A. Köhler, D.A. dos Santos, D. Beljonne, Z. Shuai, J.-L. Brédas, A.B. Holmes, A. Kraus, K. Müllen and R.H. Friend, *Nature*, **392**, 903–906 (1998).

69. N.S. Sariciftci, *Prog. Quant. Electr.*, **19**, 131–159 (1995).

70. U. Mizrahi, I. Shtrichman, D. Gershoni, E. Ehrenfreund and Z.V. Vardeny, *Synth. Met.*, **102**, 1182–1185 (1999).

71. J.-S. Kim, P.K.H. Ho, C.E. Murphy, N. Baynes and R.H. Friend, *Adv. Mater.*, **14**, 206–209 (2002).

72. J.-S. Kim, P.K.H. Ho, C.E. Murphy, A.J.A.B. Seeley, I. Grizzi, J.H. Burroughes and R.H. Friend, *Chem. Phys. Lett.*, **386**, 2–7 (2004).

73. S. Sakamoto, M. Okumura, Z. Zhao and Y. Furukawa, *Chem. Phys. Lett.*, **412**, 395–398 (2005).

74. T. Sugiyama, Y. Furukawa and H. Fujimura, *Chem. Phys. Lett.*, **405**, 330–333 (2005).

75. Y. Furukawa, M. Ishima, T. Noguchi and T. Ohnishi, *Synth. Met.*, **121**, 1649–1650 (2001).

76. Y. Furukawa, S. Furukawa, S. Maekawa and M. Ishima, *Macromol. Symp.*, **184**, 99–106 (2002).

77. G. Horowitz, *J. Mater. Res.*, **19**, 1946–1962 (2004).

78. H. Takao and Y. Furukawa, *Chem. Lett.*, **32**, 1168–1169 (2003).

79. Y. Furukawa, J. Yamamoto, D.-C. Cho and T. Mori, *Macromol. Symp.*, **205**, 9–17 (2004).

80. T. Koyanagi, M. Muratsubaki, Y. Hosoi, T. Shibata, K. Tsutsui, Y. Wada and Y. Furukawa, *Chem. Lett.*, **35**, 20–21 (2006).

81. H. Tsuji and Y. Furukawa, *Mol. Cryst. Liq. Cryst.*, **455**, 347–353 (2006).

82. T. Koyanagi, S. Furukawa, K. Tsutsui, Y. Wada and Y. Furukawa, *Vib. Spectrosc.*, **42**, 156–160 (2006).